

Liquid-Phase Citral Hydrogenation over SiO₂-Supported Group VIII Metals

Utpal K. Singh and M. Albert Vannice

Department of Chemical Engineering, Pennsylvania State University, University Park, Pennsylvania 16802-4400

Received August 11, 2000; revised December 6, 2000; accepted December 19, 2000; published online February 27, 2001

Liquid-phase citral hydrogenation over SiO₂-supported Group VIII metals at 300 K and 1 atm was studied in the absence of all transport limitations as verified by the Madon–Boudart test and the Weisz–Prater criterion. The initial TOF (turnover frequency) for citral hydrogenation varied by three orders of magnitude and exhibited the following trend: Pd > Pt > Ir > Os > Ru > Rh > Ni > Co ≫ Fe (no activity was detected over Fe/SiO₂). When TOF is correlated with percentage d-character, a volcano plot results. There are significant differences in product distribution among the different metals, with Os, Ru, and Co exhibiting high selectivity toward the unsaturated alcohol isomers (geraniol and nerol), while Rh, Ni, and Pd were more selective for citronellal and isopulegol. The variation in product distribution among the various metals is rationalized on the basis of the d-band widths that affect the relative importance of the stabilizing two-electron interactions and destabilizing four-electron interactions. With the exception of Ni/SiO₂, all catalysts exhibited substantial deactivation that was attributed to inhibition by adsorbed CO produced by the decomposition of either citral or the unsaturated alcohol. In contrast, Ni/SiO₂ exhibited an initially low, stable TOF during the first 7 h that then increased fourfold and again remained constant to 84% citral conversion, at which point the run was terminated. © 2001 Academic Press

INTRODUCTION

α,β -Unsaturated aldehydes represent a broad class of industrially relevant compounds useful in the specialty and fine chemicals industry, and hydrogenation of these compounds is of both industrial and fundamental interest (1, 2). Citral (3,7-dimethyl-2,6-octadienal) was chosen here as a probe molecule to study liquid-phase hydrogenation of α,β -unsaturated aldehydes because it has three unsaturated bonds including conjugated C=O and C=C bonds as well as an isolated C=C bond. Our investigation to date has focused on understanding the influence of reaction parameters (3, 4), crystallite size effects (5, 6), and metal–support interactions (7) on the kinetics of citral hydrogenation.

Some researchers previously have studied metal specificity related to liquid-phase α,β -unsaturated aldehyde hydrogenation, with most of the work done using crotonaldehyde and cinnamaldehyde as reactants. The work to date has been cited and summarized in a recent review by Gallezot and Richard (1). In general Os, Ru, and, to a

smaller extent, Pt favor C=O bond hydrogenation (8–11), while Ni and Pd were more selective for C=C bond hydrogenation (12–14). The differences among Group VIII metals have been addressed by the theoretical work of Delbecq and Sautet (15) as well as the density functional theory calculations of Pallassana and Neurock (16). The extended Huckel calculations of Delbecq and Sautet, in particular, suggest that the narrower the width of the metal d-band, the greater the interaction of the metal surface with the conjugated olefinic bond compared to the carbonyl bond (15).

Figure 1 displays the reaction network during citral hydrogenation over supported Group VIII metals. Thermodynamic calculations indicate that the isolated C=C bond should be the easiest to hydrogenate followed by the conjugated C=C bond and, finally, the C=O bond (17). By altering the metal, different geometric and electronic parameters are introduced that affect adsorption and reaction; thus a wide variation in reaction rate and product distribution can exist. In the present study, citral hydrogenation is examined over SiO₂-supported Group VIII metals at 300 K and atmospheric pressure, with particular emphasis on obtaining specific activities in the form of turnover frequencies (TOFs) under differential conditions free of mass transfer limitations. The product distributions varied significantly and the initial TOF varied by three orders of magnitude among these nine metals, and the latter property exhibited a maximum when correlated with the percentage d-character (18).

EXPERIMENTAL

a. Catalyst Preparation and Characterization

Davison grade 57 silica gel (220 m²/g) was dried and calcined at 773 K for 2 h prior to impregnation. The η -Al₂O₃ support was prepared by calcination of β -alumina trihydrate (Exxon Research and Engineering Co., 245 m²/g) at 873 K for 4 h. The catalysts were prepared using an incipient wetness technique by impregnating the dry calcined support with the following precursors: Fe(NO₃)₃·9H₂O (Alfa Aesar, 99.999%), Co(NO₃)₃·xH₂O (Alfa Aesar, 99.998%), Ni(NO₃)₃·6H₂O (Alfa Aesar, 99.995%), RuCl₃·xH₂O (Aldrich, 99.98%), RhCl₃·xH₂O (Aldrich,

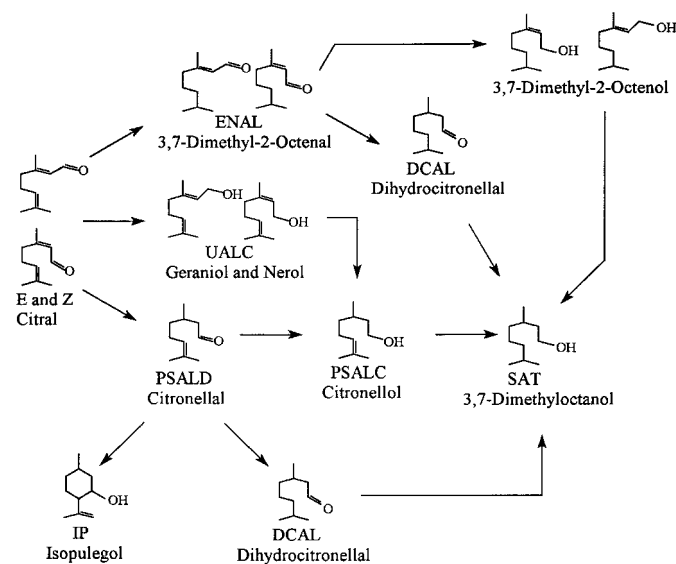


FIG. 1. Reaction network for citral hydrogenation over Group VIII metals.

99.98%), PdCl₂ (Strem, 99.9%), OsCl₃ · xH₂O (Aldrich, 99.9%), IrCl₃ · 3H₂O (Alfa Aesar, 99.9%), H₂PtCl₆ · H₂O (Aldrich, 99.995%). A 3.8% Pt/SiO₂ catalyst was prepared using an ion-exchange technique with Pt(NH₃)₄Cl₂ (Aldrich, 99.9%) as the precursor, as described elsewhere (19). The catalysts were dried overnight at 393 K and stored in a desiccator. With the exception of Pt/SiO₂, which

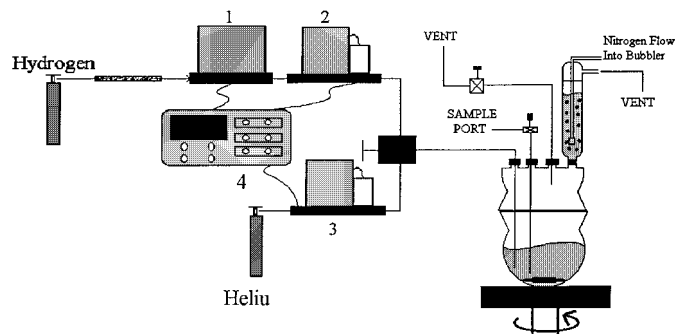


FIG. 2. Low-pressure reaction system for studying citral hydrogenation at atmospheric pressure: (1) pressure controller, (2) mass flow sensor, (3) mass flow controller, (4) modular control unit.

was reduced at 673 K, all catalysts were reduced at 723 K using the reduction times listed in Table 1. H₂ and CO chemisorption was measured on all catalysts at 300 K using the dual isotherm method (20). Dispersions and TOFs were calculated based on the total H₂ uptake except for Pd, for which the irreversible H₂ uptake was used because bulk hydride formation prevented use of the total uptake.

b. Catalytic Hydrogenation

A glass reactor system was built to study liquid-phase citral hydrogenation at 300 K and atmospheric pressure, as shown in Fig. 2. The reactor system had three unique

TABLE 1
H₂ and CO Chemisorption at 300 K and Initial Activity at 300 K, 103 kPa H₂, and 0.6 M Citral in Hexane for SiO₂-Supported Group VIII Metals

Catalyst	Precursor	<i>T</i> _{reduction} /Time	H ₂ uptakes (μmol g · cat)			H/M	Initial activity (μmol/g cat/min)	Initial TOF (1000 s ⁻¹)
			(H ₂) _{total}	(H ₂) _{rev}	(H ₂) _{irr}			
8.06% Fe/SiO ₂	Fe(NO ₃) ₃	723 K/20 h	3.5	3.0	0.5	0.005	ND	ND
8.06% Fe/SiO ₂	Fe(NO ₃) ₃	calc 623 K/1 h red 723 K/1 h	0.2	0.2	0.0	0.0003	ND	ND
8.06% Fe/SiO ₂	Fe(NO ₃) ₃	calc 623 K/1 h red 723 K/1 h <i>T</i> = 423 K	2.9	1.6	1.3	0.004	ND	ND
7.90% Co/SiO ₂	Co(NO ₃) ₃	723 K/15 h	8.9	6.6	2.3	0.01	0.1	0.10
7.90% Co/SiO ₂	Co(NO ₃) ₃	723 K/3 h	11.7	8.7	3.0	0.01	0.4	0.25
6.49% Ni/SiO ₂	Ni(NO ₃) ₂	723 K/15 h	27.7	7.5	20.2	0.05	2.4	0.7
6.49% Ni/SiO ₂	Ni(NO ₃) ₂	723 K/1 h	34.8	13.0	21.8	0.06	1.6	0.4
0.75% Ru/SiO ₂	RuCl ₃	723 K/1 h	6.3	3.6	2.7	0.17	1.6	2.1
0.43% Rh/SiO ₂	RhCl ₃	723 K/1 h	7.6	4.0	3.6	0.36	1.3	1.4
1.58% Pd/SiO ₂	PdCl ₂	723 K/1 h	32.5	29.5	2.6	0.04	37.4	120
0.08% Pd/η-Al ₂ O ₃	PdCl ₂	723 K/1 h	2.4	0.9	1.5	0.40	25.2	140
0.94% Pd/η-Al ₂ O ₃	PdCl ₂	723 K/1 h	41.3	19.3	22.0	0.50	39.6	150
1.20% Pd/η-Al ₂ O ₃	PdCl ₂	723 K/1 h	34.5	20.0	14.5	0.26	1042	598
<1% Os/SiO ₂	OsCl ₃	723 K/1 h	3.0	2.6	0.4	—	1.0	2.7
<1% Ir/SiO ₂	IrCl ₃	723 K/1 h	17.4	8.9	8.5	—	8.4	4.0
1.44% Pt/SiO ₂	H ₂ PtCl ₆	673 K/1 h	5.6	3.4	2.2	0.15	—	—
3.08% Pt/SiO ₂	Pt(NH ₃) ₄ Cl ₂	673 K/1 h	64.1	24.6	39.5	0.66	108	18.0

Note. ND, not detected.

features that deserve mention, i.e., *in situ* catalyst reduction under flowing hydrogen, degassing of hexane and citral with N_2 to remove trace quantities of dissolved oxygen, and a stirring magnet rotated by a magnetic housing connected via a flexible shaft to a high-speed motor capable of reaching stirring rates in excess of 5000 rpm. Approximately 0.5 to 1.0 g catalyst was charged into the reactor, which was then sealed, leak tested, and purged with 200 sccm He for 3 h prior to a 60-min ramp to the desired reduction temperature. Once the reduction temperature was reached, 200 sccm H_2 was purged through the reactor for 75 min prior to cooling to room temperature in hydrogen. A graduated vessel connected to one of the ports on the reactor was filled with 2 ml citral (Sigma, 97–35% neral, 65% geranial) and 240 ml of hexane (Fisher, Optima Grade). Nitrogen (MG Industries) was passed through hydrocarbon and moisture traps (Alltech) and bubbled through the citral/hexane mixture in this holding vessel for 30 min; then 200 ml of this degassed mixture was introduced into the reactor and stirring was commenced. The standard reaction conditions used in the present study were 300 K, 15 psia H_2 (103.3 kPa), and 0.06 M citral in hexane. The pressure was maintained to within 0.5 psia of the set point with a Brooks 5866 pressure controller connected to a Brooks 5860E mass flow sensor. Reaction progress was monitored by taking periodic liquid samples that were analyzed using a H-P 5890 gas chromatograph.

RESULTS

Table 1 lists the H_2 and CO chemisorption results at 300 K with these supported Group VIII metals. The Fe, Co, and Ni catalysts were prepared using nitrate precursors and high metal loadings to obtain large crystallites, facilitate metal reducibility, and minimize the influence of metal–support interactions that can occur in such systems (21, 22). Fe/SiO₂ did not adsorb hydrogen irreversibly at 300 K regardless of pretreatment conditions; however, Fe⁰ was present after calcination at 623 K and reduction at 723 K for 1 h as evidenced by CO chemisorption at 193 K and H_2 chemisorption at 423 K, both of which are techniques that are capable of detecting Fe⁰ surface atoms (23, 24). In addition, Mössbauer spectra indicated the presence of large Fe⁰ particles after reduction at 723 K for 20 h, exposure to air, and then another reduction at 673 K for 1 h (25).

Prior to evaluating reaction kinetics, it was important to ensure that all transport limitations were absent by application of the Madon–Boudart test (26). Figure 3 shows a ln–ln plot of activity vs Pd_s concentration over a family of SiO₂- and η -Al₂O₃-supported Pd catalysts in which the concentration of surface Pd atoms, Pd_s, obtained from the irreversible H_2 uptake at 300 K, varied more than 20-fold from 3 to 66 μ mol Pd_s/g cat. A slope near unity was obtained within experimental uncertainty indicating the absence of

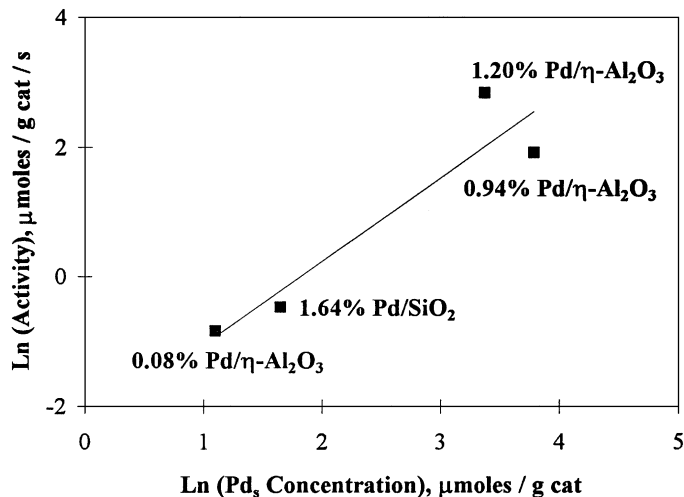


FIG. 3. Madon–Boudart test with a family of Pd catalysts at 300 K, 103 kPa H_2 , and 0.06 M citral in hexane.

any mass transfer limitations in the kinetic data. Application of the Madon–Boudart test at two different reaction temperatures can ensure that heat transfer, as well as mass transfer, limitations are absent; however, as discussed later, application of this test at one temperature is sufficient to verify the absence of transport limitations in the present case.

Figure 4 shows the temporal citral conversion profile during hydrogenation over 0.5 g of 3.8% Pt/SiO₂ at standard conditions. With the exception of Ni/SiO₂, all catalysts exhibited an initial rate followed by a substantial decrease in activity. This deactivation complicated the evaluation of reaction rates; therefore, a standard procedure for evaluating rates was developed by fitting the temporal

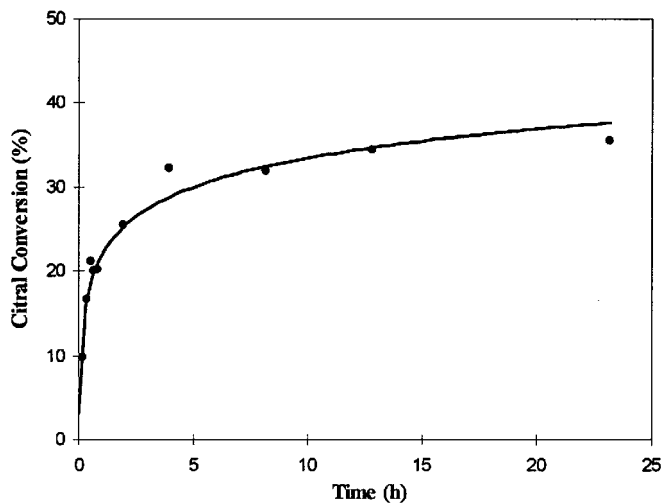


FIG. 4. Temporal citral conversion profile for citral hydrogenation over 3.80% Pt/SiO₂ at 300 K, 103 kPa H_2 , and 0.06 M citral in hexane.

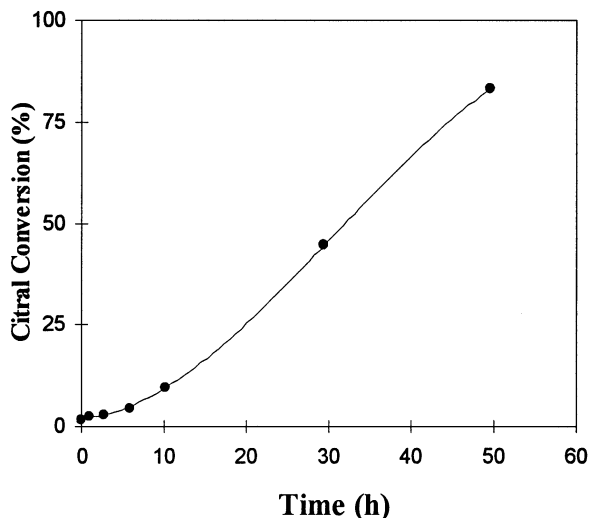


FIG. 5. Temporal citral conversion profile for citral hydrogenation over 6.49% Ni/SiO₂ at 300 K, 103 kPa H₂, and 0.06 M citral in hexane.

citral conversion profile to a logarithmic profile and determining the rate based on the derivative of the profile at 5% citral conversion. For example, the temporal citral conversion profile for reaction over Ru/SiO₂ was fit by $3.0139 * \ln(\text{time}) + 1.9002$, and the TOF at 5% conversion was 0.0021 s^{-1} . Ni/SiO₂ was the one catalyst that exhibited substantially different kinetics because the initial TOF for citral disappearance remained constant at 0.0007 s^{-1} for the first 7 h of reaction and then increased fourfold to 0.003 s^{-1} and again remained constant up to 80% citral conversion. This is shown in Fig. 5.

Table 2 displays the product distributions at 5% conversion during citral hydrogenation at standard conditions over the SiO₂-supported catalysts. With the exception of Pt, none of the catalysts produced citronellol. Furthermore, none of these catalysts produced detectable amounts of dihydrocitronellal or the completely saturated product (3,7-dimethyloctanol) at 5% citral conversion. The Pt/SiO₂ catalyst produced 23% citronellol and 50% citronellal. The

most selective metal for C=O bond hydrogenation was Os, which gave nearly 90% selectivity to the unsaturated alcohol isomers (geraniol + nerol) with the remainder being citronellal. Both Ru/SiO₂ and Co/SiO₂ gave approximately 55% unsaturated alcohol with about 30% citronellal and 15% isopulegol constituting the balance of the products. Pd and Ni catalysts exhibited the highest initial selectivity to citronellal, i.e., approximately 70%. The selectivities tabulated in Table 2 represent a snapshot of the reaction mixture at only one citral conversion; thus it is important to examine the selectivity vs conversion behavior in greater detail to better understand metal specificity. Figure 6 displays the cumulative selectivity vs conversion plots for all the SiO₂-supported Group VIII metals, and the results are arranged in order of the metal's location in the periodic table. No product distribution is displayed for Fe/SiO₂ due to the negligible activity observed during reaction. The cumulative selectivity is defined as

$$S_i = \frac{C_i}{\sum_{\text{Products}} C_i},$$

where C_i is the concentration of species i . The range of conversion encompassed by the various metals varies from approximately 10% over Rh and Os to nearly 100% over Ni catalysts. This difference is attributed to greater deactivation with some of the catalysts, especially those at low loadings.

DISCUSSION

Mass Transfer and Crystallite Size Effects

The influence of mass transfer effects was evaluated by the application of the Madon–Boudart test at 300 K to test for internal and external mass transfer limitations (26). Application of this test at two different temperatures can ensure that neither heat nor mass transfer limitations affect the data. However, it has been shown earlier that temperature gradients are lower in liquid–solid systems,

TABLE 2

Product Distribution at 5% Citral Conversion over SiO₂-Supported Group VIII Metals during Reaction at 300 K, 103 kPa H₂, and 0.06 M Citral in Hexane

Catalyst	Geraniol + nerol	Citronellal	Isopulegol	Citronellol	3,7-Dimethyl- 2-octenal	Dihydrocitronellal	3,7-Dimethyloctanol
8.06% Fe/SiO ₂	—	—	—	—	—	—	—
7.90% Co/SiO ₂	55	30	15	0	0	0	0
6.49% Ni/SiO ₂	0	61	39	0	0	0	0
0.75% Ru/SiO ₂	56	27	17	0	0	0	0
0.43% Rh/SiO ₂	0	74	26	0	0	0	0
1.58% Pd/SiO ₂	0	69	7	0	24	0	0
Os/SiO ₂	88	12	0	0	0	0	0
Ir/SiO ₂	0	52	34	0	14	0	0
3.8% Pt/SiO ₂	0	50	12	23	15	0	0

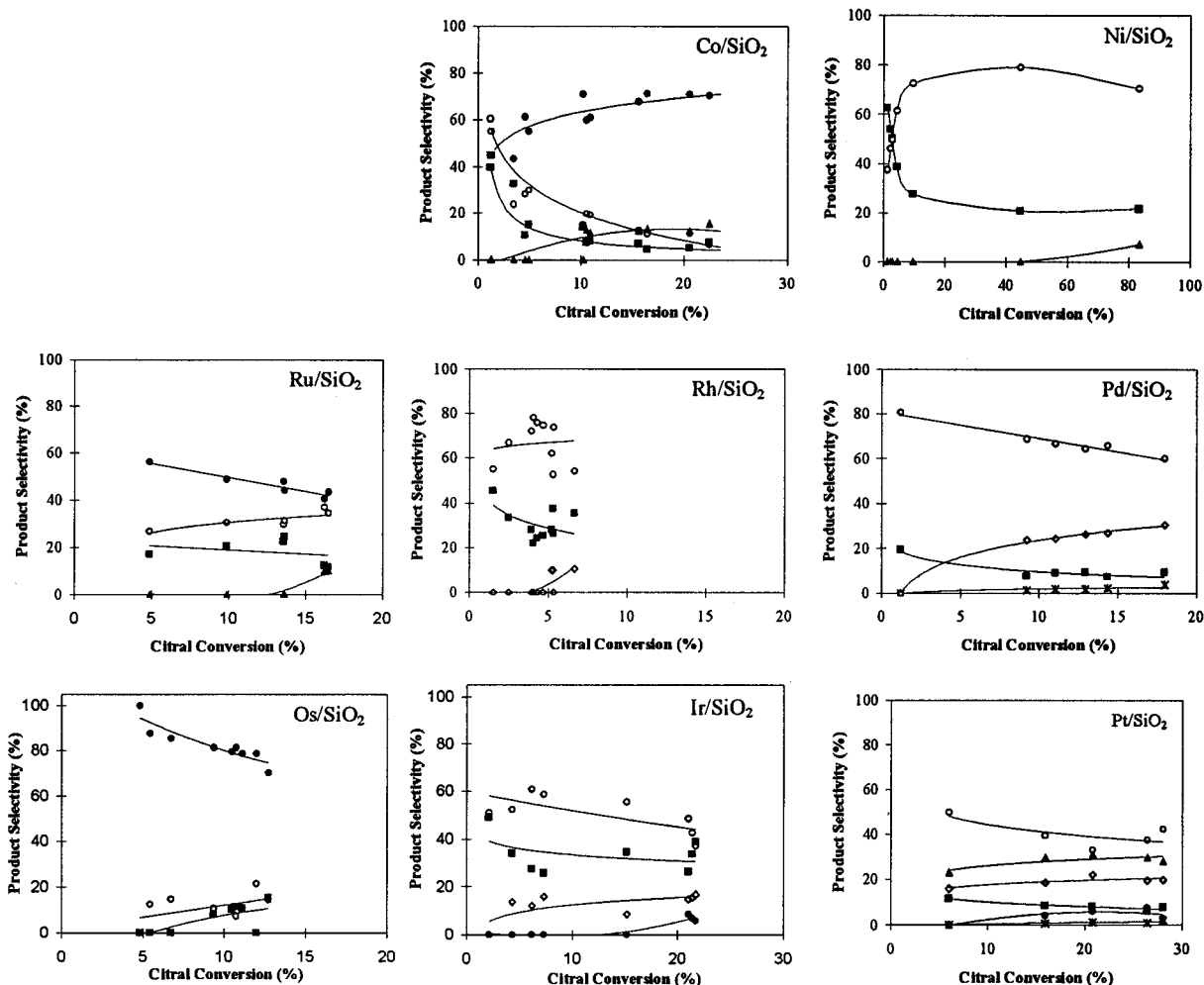


FIG. 6. Product distribution exhibited by SiO₂-supported Group VIII metals during citral hydrogenation at 300 K, 103 kPa H₂, and 0.06 M citral in hexane. Figures are arranged in order of the metal location in the periodic table of elements. (●) geraniol plus nerol, (○) citronellal, (■) isopulegol, (*) dihydrocitronellal, (▲) citronellol, (◇) 3,7-dimethyl-2-octenal.

compared to gas–solid systems, due to the higher heat capacities and thermal conductivities in the former (7). Moreover, internal diffusion limitations were also shown to be absent by applying the Weisz–Prater parameter (27) to a 1.58% Pd/SiO₂ catalyst, which gave a value of 0.002 and assured the absence of internal diffusion limitations. Therefore, all these results indicate the absence of any transport limitations from the kinetic data reported here.

It should be mentioned that crystallite size effects are not expected to have a significant influence on the differences in the kinetics among the various metals. Mercadante *et al.* have shown that citral hydrogenation over Ru/Al₂O₃ is structure insensitive at 333 K (11). We have previously shown that the crystallite size effect observed at 373 K and 20 atm H₂ with Pt/SiO₂ was not observed during reaction at 300 K (5). Furthermore, no crystallite size effect was observed with supported Pd catalysts, as shown in Table 1 for a family of Pd/SiO₂ and Pd/η-Al₂O₃ catalysts in which

the dispersion varied from 0.04 for 1.58% Pd/SiO₂ to 0.60 for 1.20% Pd/η-Al₂O₃. The TOFs on 0.08% Pd/η-Al₂O₃ (H_{irr}/Pd = 0.40), 0.94% Pd/η-Al₂O₃ (H_{irr}/Pd = 0.50), 1.58% Pd/SiO₂ (H_{irr}/Pd = 0.04), and 1.2% Pd/η-Al₂O₃ (H_{irr}/Pd = 0.60) are 0.14, 0.15, 0.12, and 0.59 s⁻¹, respectively. These results imply the absence of any significant crystallite size effects at 300 K. In addition, the product distribution was also unaffected by crystallite size for citral hydrogenation over Pt/SiO₂, Pd/SiO₂, and Ru/Al₂O₃ catalysts (5, 11). Therefore, the product distributions over the Group VIII metals reported in the present study are presumed to be unaffected by crystallite size effects.

Catalyst Deactivation

The deactivation behavior exhibited by Pt/SiO₂ (Fig. 4), as well as Ru, Rh, Pd, Os, Ir, and Co, is consistent with the behavior observed during high pressure citral

hydrogenation over Pt/SiO₂ at 300 K, which was attributed to a decarbonylation reaction yielding adsorbed CO that blocked active sites (3). There are spectroscopic studies of Pt, Pd, Ru, and Rh surfaces that clearly indicate the presence of adsorbed CO during adsorption and decomposition of unsaturated aldehydes and alcohols (28–33). Based on such spectroscopic evidence as well as several kinetic studies, unsaturated alcohol decomposition was suggested to be responsible, at least in part, for the deactivation behavior (3, 4). The deactivation exhibited by Rh and Pd in the absence of the unsaturated alcohol suggests that citral decomposition may also occur on some metals during the hydrogenation reaction. Citronellal decomposition is not a likely source of the deactivation because surface science studies by Davis and Barteau have shown that the presence of a vinyl substituent adjacent to the C=O bond in acrolein results in it having a lower activation barrier for decarbonylation compared to propanal (31). In addition, a DRIFTS study of citral, citronellal, and geraniol decomposition indicated that citral and geraniol decarbonylation occurred at a lower temperature compared to that of citronellal (25). The deactivation behavior observed over these metal surfaces indicates that the decomposition reaction occurs at relatively low temperatures, i.e., 300 K, which is consistent with the work of de Jesus and Zaera which has shown that most of the decarbonylation of acrolein and crotonaldehyde on Pt (111) occurs between 250 and 340 K (28).

In addition to spectroscopic studies with single crystal surfaces, Lercher and coworkers (34) have found indirect evidence for CO involvement in the deactivation process during liquid-phase crotonaldehyde hydrogenation over Pt/SiO₂. They observed temporal conversion profiles similar to the profile shown in Fig. 4. When a completely deactivated catalyst was purged with O₂ to oxidize adsorbed CO to CO₂, the initial activity prior to the deactivation was retained (34). Figure 7 displays similar results for citral hydrogenation over 3.80% Pt/SiO₂ at 300 K and 103 kPa H₂. An initial TOF of 0.016 s⁻¹ was obtained followed by substantial deactivation yielding a 20-fold lower TOF of 0.0008 s⁻¹ after 4 h of reaction. Purging the reactor with air and reintroducing H₂ produced a TOF of 0.015 s⁻¹, thus regaining the activity at the start of the reaction. In agreement with the results of Lercher and coworkers, this procedure restored the initial activity but did not affect the product distribution. Since the oxidation treatment was performed at 300 K, the oxidation of carbonaceous species is not expected because such processes require higher temperatures (35). Furthermore, the carbonaceous species resulting from the decarbonylation reaction are rapidly hydrogenated and desorbed from the surface (36, 37). The inhibiting effect of CO was also shown by the following experiment. The catalyst was purged with He for 2 h at 673 K after the reduction step and cooled to room temperature in He, and then CO was adsorbed on the catalyst at 300 K prior to the addition

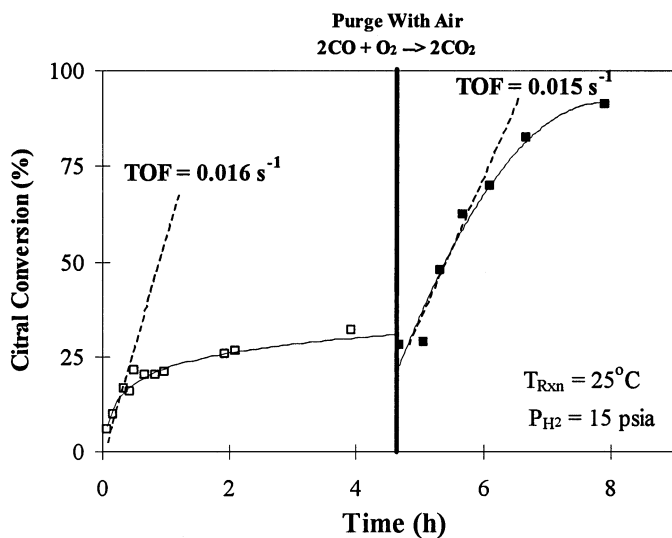


FIG. 7. Temporal citral conversion profile for citral hydrogenation over 3.80% Pt/SiO₂ at 300 K, 103 kPa H₂, and 0.06 M citral in hexane. Air (1000 sccm) was purged through the reactor at 300 K after 5 h of reaction to restore the initial activity.

of citral and hexane to start the reaction. A comparison of the temporal citral conversion profiles is shown in Fig. 8. The CO-inhibited catalyst exhibits an order of magnitude lower TOF compared to the catalyst that had not been exposed to CO. Since studies with single crystal Rh, Pd, and Pt surfaces (28–31) and SiO₂-supported Ru and Co catalysts (32, 33, 38) have shown the presence of a decarbonylation reaction during the adsorption of α,β -unsaturated aldehydes, it is reasonable to expect that the decarbonylation reaction proposed for Pt/SiO₂ deactivation can also occur on SiO₂-supported Rh, Pd, Ru, and Co. Toroude has shown

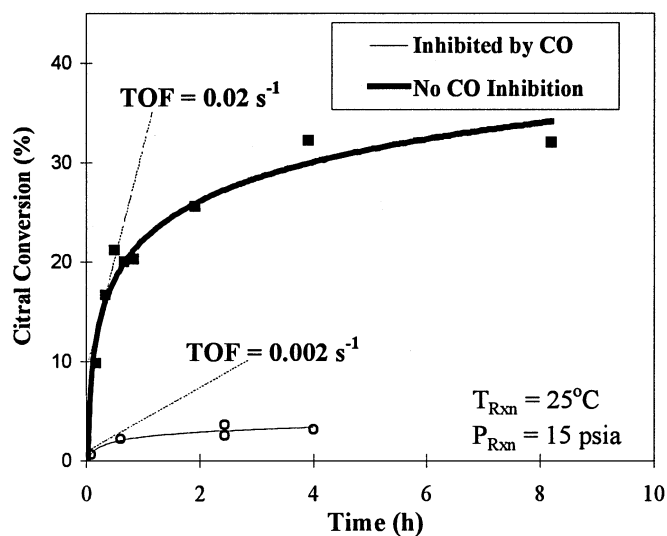


FIG. 8. Influence of CO adsorption prior to reaction on the temporal citral conversion profile for hydrogenation over 3.80% Pt/SiO₂ at 300 K, 103 kPa H₂, and 0.06 M citral in hexane.

TABLE 3

Total Number of Turnovers (TNT) during Citral Hydrogenation over SiO₂-Supported Group VIII Metals at 300 K, 103 kPa H₂, and 0.06 M Citral in Hexane

Metal	Total number of turnovers
8.06% Fe/SiO ₂	— ^a
7.90% Co/SiO ₂	32 ^b
6.49% Ni/SiO ₂	61 ^c
0.75% Ru/SiO ₂	25.5
0.43% Rh/SiO ₂	7.1
1.58% Pd/SiO ₂	138.5
Os/SiO ₂	196.0
Ir/SiO ₂	12.6
3.8% Pt/SiO ₂	8.3

^aNo activity detected.

^bSlow deactivation. Plateau was not reached.

^cNo deactivation was observed.

acrolein decarbonylation on Co, Rh, and Fe; therefore, CO inhibition may also exist on these catalysts (9). Although alternative inhibition mechanisms, such as C–O bond hydrogenolysis, have been suggested to occur on various metals (9, 36), and they cannot be discounted at this time, the results presented in Figs. 7 and 8 in conjunction with earlier studies (3, 5) argue strongly in favor of the decarbonylation reaction as the source of the deactivation.

Table 3 lists the total number of turnovers (TNT), defined as the moles of citral converted per mole of surface metal atom, prior to complete deactivation. The TNT was evaluated using the conversion at the plateau of the temporal citral conversion profile, i.e., 35% for the profile in Fig. 4. The results presented for Co/SiO₂ must be taken with caution due to the slower deactivation exhibited by this catalyst which prevented the plateau-like behavior from being realized in the time span of the experiment. However, it should be stressed that the Co/SiO₂ also exhibited deactivation during the course of the reaction. Furthermore, the TNT value listed for Ni/SiO₂ was calculated using 84% conversion, the maximum conversion observed, since no deactivation occurred during reaction. No correlation of the TNT with percentage d-character or d-band width could be found. Pt and Rh have the lowest TNT, and therefore it may be argued that these catalysts have a greater propensity for the decarbonylation reaction compared to SiO₂-supported Pd and Os, which exhibit TNT values that are more than an order of magnitude higher. It is difficult to rationalize the differences in TNT among the various metals since they reflect inhibition arising from citral or unsaturated alcohol decomposition, and the mechanistic details of these reactions vary among the Group VIII metals (39). Barteau and coworkers have suggested that ethanol decomposition on Rh occurs through an oxametallacycle intermediate (30), compared to an aldehyde intermediate on Pt, Pd, and Ni sur-

faces (39–42). Furthermore, while Davis and Barteau observed hydrocarbon desorption during ethanol decomposition over Pd (40), no such products were observed during ethanol decomposition over Pt and Rh (30, 41). In addition to the mechanistic variation of the decomposition reaction, Shekhar and Barteau have shown that the alcohol decomposition reaction is structure sensitive on Pd (43), which introduces another parameter in the deactivation mechanism that may help explain the differences in the total number of turnovers exhibited by the Group VIII metals in the present study.

The temporal concentration profile over Ni/SiO₂ differs markedly from the profiles with the other active metals, as shown in Fig. 5. Similar behavior is also apparent in the results of Tiainen *et al.* for citral hydrogenation at atmospheric pressure over a Ni/Al₂O₃ catalyst (14), although it was not explicitly stated, and their results also suggest a decrease in reaction rate with increasing temperature similar to the behavior observed with Pt/SiO₂. The kinetics of citral hydrogenation over Ni/SiO₂ exhibit two regimes, as shown by the temporal citral conversion and the instantaneous citronellal selectivity profiles in Fig. 9. The instantaneous selectivity is defined as

$$S_i^{\text{INST}} = \frac{r_i}{\sum_{\text{Products}} r_i},$$

where r_i is the rate of each step in Fig. 1. This parameter is a more accurate representation of instantaneous changes in product distribution during reaction (5). The low initial TOF of 0.0007 s⁻¹ observed during the first 7 h of reaction up to 10% conversion is accompanied by an increase in the

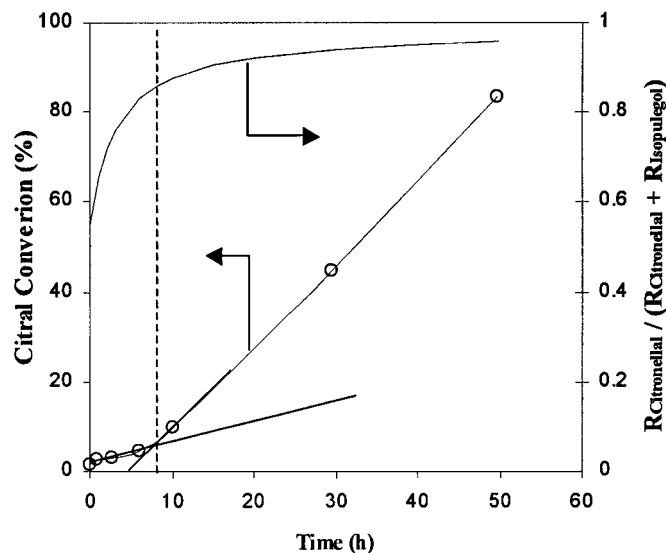


FIG. 9. Temporal citral conversion profile and instantaneous selectivity to citronellal during citral hydrogenation over 6.49% Ni/SiO₂ at 300 K, 103 kPa H₂, and 0.06 M citral in hexane. Dotted line denotes change in trend.

instantaneous selectivity to citronellal from 60% initially to 90% after 7 h of reaction. Subsequently, the temporal citral conversion profile exhibits a fourfold enhancement in TOF with a near zero-order dependence on citral that is accompanied by a 95% instantaneous selectivity to citronellal up to citral conversions greater than 80%.

Since complete reduction of SiO₂-supported Fe, Co, and Ni catalysts can be difficult, it is tempting to suggest that the increase in rate during reaction may be related to further reduction of Co and Ni during reaction. However, this is not believed to be the case for the following reasons. Mössbauer results revealed large Fe⁰ crystallites and no Fe²⁺ or Fe³⁺ species in the 8.06% Fe/SiO₂ catalyst after reduction at 723 K for 20 h, exposure to air at room temperature, and re-reduction *in situ* at 673 K for 1 h. The absence of bulk oxide in Fe/SiO₂, even after exposure to air and reduction at 673 K for only 1 h, suggests that a Ni/SiO₂ catalyst undergoing an identical pretreatment should also have only Ni⁰ in the bulk. Furthermore, H₂ chemisorption at 300 K clearly reveals the presence of Ni⁰ at the surface. In view of the above results, the increase in rate during reaction on Ni/SiO₂ should not be due to additional reduction under reaction conditions, but is more likely due to kinetic factors. It is our hypothesis that the initial induction period involves competitive adsorption and reaction of impurities in citral, which was obtained commercially with a purity of 97%. To test this explanation, the experiment shown in Fig. 10 was conducted. This figure displays the temporal citral conversion profile for citral hydrogenation over 6.49% Ni/SiO₂ under standard conditions. The TOF during the initial induction period was 0.0011 s⁻¹, after which time a TOF of 0.0028 s⁻¹ was measured. Addition of another 0.40 g of freshly reduced catalyst resulted in a similar TOF of 0.0036 s⁻¹. This is exactly what would be expected if the initial induction period were due to the competitive hydro-

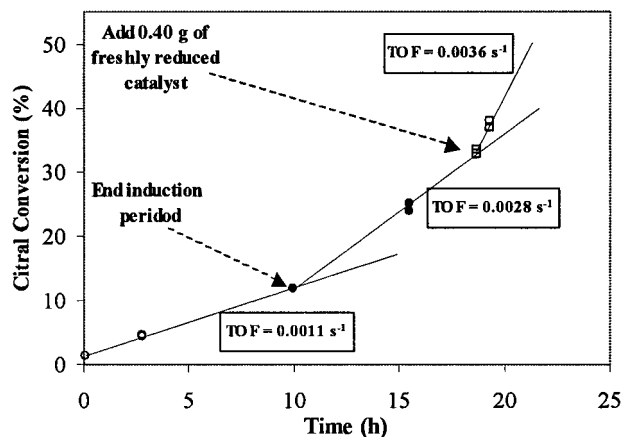


FIG. 10. Temporal citral conversion profile for reaction over 0.45 g 6.49% Ni/SiO₂ at 300 K, 103 kPa H₂, and 0.06 M citral in hexane. Freshly reduced 6.49% Ni/SiO₂ (0.40 g) was added after 19 h of reaction.

TABLE 4

Effect of H₂ Pressure on TOF and Product Distribution (at 20% Citral Conversion) during Citral Hydrogenation over Pt/SiO₂ at 300 K

	1 atm H ₂ ^a	20 atm H ₂ ^b
TOF (s ⁻¹)	0.018	0.19
Geraniol + nerol	10	10
Citronellal	32	38
Isopulegol	12	4
Citronellol	23	23
3,7-Dimethyl-2-octenal	23	18
Dihydrocitronellal	0	2
3,7-Dimethyloctanol	0	5

^a Reaction was conducted over 3.8% Pt/SiO₂ catalyst at 300 K, 15 psia H₂, with 0.06 M citral in hexane.

^b Reaction was conducted over 1.4% Pt/SiO₂ catalyst at 300 K, 20 atm H₂, with 1 M citral in hexane.

genation and removal of impurities in the feed that inhibit the reaction. This result argues against Ni surface modification under reaction conditions as a cause for the initial rate increase. At this stage, it is unclear why Ni appears to be the most susceptible to feed impurities, and detailed kinetics in the form of temperature dependence and reaction orders are required to better understand this behavior.

No significant activity could be detected over the 8.06% Fe/SiO₂ sample used in the present study. This is not surprising in view of Touroude's gas-phase results for acrolein hydrogenation and deuteration over supported Group VIII metals. He attributed the low deuterium-acrolein activity on iron to carburation of the catalyst based on similar results obtained with butadiene (9).

Pressure Effects

Pressure effects in such reactions have been noted (1), but a comparison of the product distribution at 1 atm over Pt/SiO₂ at 20% citral conversion in the present study with that obtained earlier for citral hydrogenation at 300 K and 20 atm H₂ (3) reveals no significant pressure effect on product distribution over Pt catalysts, as shown in Table 4. One of the differences in the product distribution between reaction at 1 and 20 atm is the 5 and 2% selectivity for 3,7-dimethyloctanol and dihydrocitronellal at 20 atm. It is not surprising that the isolated and tri-substituted C=C bond is slower to hydrogenate at low pressures, and more vigorous conditions are required for its hydrogenation. Furthermore, selectivity to isopulegol is greater at 20 atm, compared to that at 1 atm, for reasons that are not clear presently. The absence of a significant pressure effect on product distribution for more than an order of magnitude increase in H₂ pressure suggests similar reaction orders with respect to H₂ pressure among the steps in the parallel reaction network of citral hydrogenation to yield the partially saturated

aldehyde (citronellal) or the unsaturated alcohol isomers (geraniol and nerol). In addition, the initial rate exhibits a near first-order dependency on H_2 pressure because the initial TOF for citral hydrogenation increased from 0.018 to 0.19 s^{-1} as the H_2 pressure increased from 1 to 20 atm.

Metal Specificity

Most of the experimental studies of α,β -unsaturated aldehyde adsorption have focused on acrolein and crotonaldehyde. Barteau and coworkers studied acrolein adsorption on single crystal Pd and Rh surfaces (29–31, 44) while de Jesus and Zaera studied crotonaldehyde and acrolein on Pt (111) (28). Cordier and coworkers examined crotonaldehyde and 3-methylcrotonaldehyde adsorbed on various Pt single crystal surfaces (37, 45, 46), while Bailie *et al.* have investigated acrolein adsorption and hydrogenation on SiO_2 -supported Co (38). Unfortunately, similar studies do not exist for citral, and detailed surface science studies of α,β -unsaturated aldehyde adsorption on Os, Ir, or Ni surfaces have not yet been reported. Nevertheless, there are some generalizations that can be made based on the experimental data and the theoretical results that have been reported.

Significant differences exist in product distribution among the different metals, as shown in Table 2 and Fig. 6. Despite the bulky substituent groups at the conjugated C=C bond of citral, metals such as Ni, Rh, and Pd are highly selective toward hydrogenation of the conjugated C=C bond and not the C=O bond. In fact, Ni exhibits an instantaneous selectivity to citronellal of nearly 95% after the initial induction period (Fig. 9). This is in contrast to what would have been expected from steric arguments that would suggest that the presence of bulky substituent groups at the conjugated C=C bond hinders adsorption via this bond and its hydrogenation, thus enhancing selectivity for C=O bond hydrogenation (10, 46, 47). Furthermore, a recent study by de Jesus and Zaera indicates that crotonaldehyde interacts with the Pt (111) surface primarily via the conjugated C=C bond, despite the methyl substituent on one of the C atoms in the conjugated C=C bond, whereas acrolein interacts with the surface primarily via the C=O bond (28). In view of these results, it appears that steric effects imposed by substituent groups on the C atoms in the C=C bond do not have as large an influence on intramolecular selectivity as the nature of the metal.

As mentioned previously and reinforced by others (16, 28), there is scant experimental data for adsorption of more complex α,β -unsaturated aldehydes, such as citral, on Group VIII metals; therefore, the adsorption behavior of such compounds is unknown. However, acrolein adsorption on Pt, Pd, and Rh surfaces has been studied in some detail (28, 29, 44). The RAIRS study of de Jesus and Zaera indicates that acrolein is coordinated parallel to the surface with primary interaction via the C=O bond (28). Similarly,

Barteau and coworkers have found that acrolein interacts with Pd and Rh via the C=O bond in a $\eta^2(C, O)$ configuration at 90 K, with subsequent rehybridization around 150–170 K to an $\eta^4(C, C, C, O)$ mode. It should be stressed that the results of de Jesus and Zaera indicate that, in contrast to acrolein, crotonaldehyde interacts with a Pt (111) surface primarily via the C=C bond, which is consistent with our results for citral hydrogenation showing that citronellal was the primary product over Pt. It is surprising that the results of Barteau and coworkers indicate that acrolein interacts with Pd and Rh in an $\eta^2(C, O)$ mode because during citral hydrogenation on Pd and Rh no products rising from C=O bond hydrogenation are formed. It may be that the differences in adsorption behavior between crotonaldehyde and acrolein on Pt (111) that were observed by de Jesus and Zaera (28) may also occur with Rh and Pd surfaces, and the C=C bond containing the most substituent groups is the one primarily interacting with the surface. Both the DFT calculations of Pallassana *et al.* (48) and the HREELS study of Xu and Goodman (49) have shown that maleic anhydride (which also contains conjugated C=C and C=O bonds) interacts with the Pd (111) surface via the C=C bond. Furthermore, theoretical studies of Re (located next to Os in the periodic table of elements) indicate that maleic anhydride interacts with the Re (0001) surface via the C=O bond (48). Assuming similar behavior for Re and Os, the theoretical results are consistent with our experimental data which show that Pd favors hydrogenation of the C=C bond whereas Os favors hydrogenation of the C=O bond. In view of the previous discussion, it is difficult to explain our results only on the basis of surface science studies because the adsorption behavior of complex α,β -unsaturated aldehydes, for which scant data exist, appears to be different from that of simpler model compounds, which prefer interaction via the C=O bond on Pt, Pd, and Rh surfaces.

Delbecq and Sautet utilized extended Huckel calculations to study adsorption of unsaturated organics on various Pt and Pd single crystal surfaces, and they have interpreted their results in terms of stabilizing two-electron interactions and destabilizing four-electron interactions, with adsorption strength and geometry determined by the balance between these interactions (15, 50, 51). The two-electron interactions involve electron transfer between the organic molecule and the metal surface and include the conventional donation and back donation processes, whereas the four-electron interactions involve destabilizing and repulsive interactions between filled states at the metal surface and the occupied molecular orbitals of the organic. It should be stressed, as the authors have themselves stated, that these results must be examined from a qualitative perspective due to the uncertainty inherent in quantitative comparisons of extended Huckel calculations; however, the arguments developed by Delbecq and Sautet for the adsorption of α,β -unsaturated aldehydes on Pt and Pd

surfaces can be utilized to rationalize the differences in product distribution between SiO₂-supported Pt and Pd catalysts in the present study, as shown in Table 2 and Fig. 6. Pd has an initial selectivity to citronellal of 80% while Pt exhibited a lower selectivity of 50% but had a selectivity of almost 25% to citronellol (hydrogenation of both conjugated C=C and C=O bonds). This is consistent with the theoretical calculations of Delbecq and Sautet which indicate that Pd exhibits reduced destabilizing four-electron interactions because of a narrower d-band width compared to Pt, thus allowing greater interaction between the conjugated C=C bond and the Pd surface. Furthermore, Ni has a narrower d-band width compared to Pd and also does not hydrogenate the C=O bond, as it exhibits an initial selectivity to citronellal of 61% with the remainder of the product resulting from the isomerization of citronellal to isopulegol, as shown in Fig. 6. The wider d-band of Pt, on the other hand, decreases interaction between the conjugated C=C bond alone and the Pt surface because of enhanced repulsive four-electron interactions that result in greater interaction between the surface and the C=O bond, thereby allowing simultaneous hydrogenation of C=O and C=C bonds. The low selectivity to the unsaturated alcohol (geraniol + nerol) suggests that citral may be adsorbed on the surface in such a manner that hydrogenation of the C=O bond occurs concurrently with the C=C bond since it is well established that kinetic factors favor hydrogenation of the C=C bond compared to the C=O bond (17, 47).

Experimental and theoretical results indicate that the width of the d-band increases going down the periodic table, i.e., moving from Fe to Os, and going from right to left, i.e., Pt to Os (52, 53), and Table 5 lists the d-band widths obtained from the XPS data of Fadley and Shirley (52). These values do not agree well with recent theoretical results (53); however, exact values are less important than the trends exhibited for the qualitative analysis that follows. In view of these trends and the rationale of Delbecq and Sautet, one would expect Os and Ru to exhibit the highest selectivity

for C=O bond hydrogenation to yield geraniol and nerol; in contrast, Ni and Pd should exhibit the highest selectivity for C=C bond hydrogenation. Rh possesses a d-band width similar to that of Pd (52); therefore, it is not surprising that the only products observed during citral hydrogenation over Rh/SiO₂ were those arising from the hydrogenation of the conjugated C=C bond to give citronellal, its isomerization, and the subsequent hydrogenation of the isolated C=C bond. This behavior is also consistent with the results of Mercadante *et al.* (11) and Wismeijer *et al.* (54) which show that Ru is selective for hydrogenation of the C=O bond in citral and citronellal. Furthermore, Rh, Pd, and Ni are known to provide excellent homogeneous and heterogeneous catalysts for C=C bond hydrogenation (12–14, 55). The results of Delbecq and Sautet have also been used by Lercher and coworkers to explain crystallite size effects during liquid-phase crotonaldehyde hydrogenation over supported Pt catalysts (56).

Although changes in product distribution are consistent with trends in d-band width, there are a number of additional factors that this model does not account for. One of these is the change in product distribution as conversion increases due to either the kinetics of competing reactions or modification of the metal surface under reaction conditions, such as that reported during hydrogenation of α,β -unsaturated aldehydes (57). The selectivity vs conversion behavior over Co and Ni catalysts represent an extreme of this behavior. The selectivity to citronellal over Ni increases from less than 40% initially to 80% at a citral conversion of 40%, whereas with Co the selectivity to the unsaturated alcohol increases from 40% at 3% conversion to 70% at 20% citral conversion. Moreover, no unsaturated alcohol is observed over Co/SiO₂ during the first hour of reaction (up to 3% conversion) and only citronellal and isopulegol were detected. Co has a d-band width similar to that of Pd and Rh; consequently it is not surprising that hydrogenation of only the conjugated C=C bond and its subsequent isomerization is observed initially, and no product due to C=O bond hydrogenation is observed. To a lesser extent, similar changes in product distribution are apparent with Ir and Pt catalysts. Both catalysts are initially unselective for hydrogenation of the carbonyl bond; however, after conversion reaches about 10%, unsaturated alcohols become detectable and attain a cumulative selectivity of around 10%. Incidentally, Ir has a large d-band width (Table 5); therefore, it is surprising that unsaturated alcohols are not detected in the initial product distribution; however, unsaturated alcohol selectivity does increase with increasing citral conversions once the latter reaches 10% (Fig. 6). In addition to changes in product distribution, this correlation with the d-band width does not account for possible changes in the activation barriers associated with different metals that was noted by Pallassana and Neurock (16).

TABLE 5

Width of the d-Band for Group VIII Metals Obtained from XPS Measurements

Metal	d-Band Width ^a (ev)
Fe	4.2
Co	4.0
Ni	3.0
Ru	4.9
Rh	4.4
Pd	4.1
Os	6.5
Ir	6.3
Pt	5.8

^a Ref. 52.

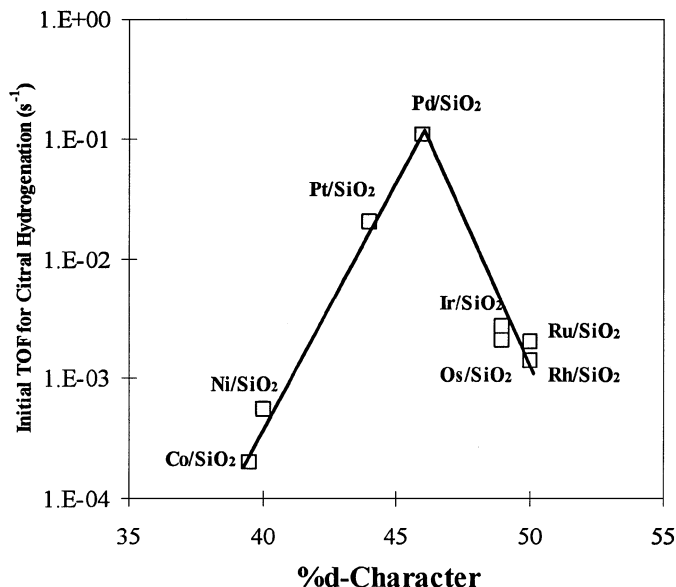


FIG. 11. Correlation of the initial TOF for citral hydrogenation with percentage d-character. TOF was evaluated under differential conditions for citral hydrogenation at 300 K, 103 kPa H₂, and 0.06 M citral in hexane.

The initial TOF varied by almost three orders of magnitude among the metals dispersed on SiO₂, with Pd exhibiting the highest TOF of 0.12 s⁻¹ and Co exhibiting the lowest detectable TOF of 0.00025 s⁻¹. As mentioned, Fe was inactive, but this lack of activity may possibly be due to very rapid deactivation. Figure 11 displays the correlation of the initial citral hydrogenation TOF over SiO₂-supported metals with the percentage d-character, which is an empirical indicator of the electronic structure of the metal (18). As the name implies, percentage d-character refers to the contribution of the d-electrons to the spd hybrid orbitals assumed in Pauling's resonance valence band theory. The correlation of activity with this parameter has been utilized before for reactions under reducing conditions (58), and Sinfelt has correlated ethane hydrogenolysis activity with this parameter (59).

SUMMARY

The initial TOF for citral hydrogenation over SiO₂-supported Group VIII metals varied by nearly three orders of magnitude at 103 kPa H₂ and 300 K, i.e., from 0.12 s⁻¹ for Pd to 0.00025 s⁻¹ for Co. The initial TOF for citral hydrogenation exhibited the following trend: Pd > Pt > Ir > Os > Ru > Rh > Ni > Co ≫ Fe. There are also significant differences in product distribution, with Os, Ru, and Co exhibiting high selectivity to the unsaturated alcohol isomers (geraniol and nerol), while Ni, Pd, and Rh exhibit high selectivity to citronellal and isopulegol. With the exception of Ni/SiO₂, all catalysts exhibited substantial deactivation due to citral and/or unsaturated alcohol decomposition to

yield adsorbed CO that poisoned active sites responsible for hydrogenation. In contrast, Ni/SiO₂ exhibited an initially low TOF that increased fourfold after 7 h of reactions after which time no deactivation was detected up to 84% conversion.

ACKNOWLEDGMENT

This study was supported by the DOE, Division of Basic Energy Sciences, under Grant DE-FE02-84ER13276.

REFERENCES

- Gallezot, P., and Richard, D., *Catal. Rev. Sci. Eng.* **40**, 81 (1998).
- Claus, P., *Top. Catal.* **5**, 51 (1998).
- Singh, U. K., and Vannice, M. A., *J. Catal.* **191**, 165 (2000).
- Singh, U. K., Sysak, M., and Vannice, M. A., *J. Catal.* **191**, 181 (2000).
- Singh, U. K., and Vannice, M. A., *Stud. Surf. Sci. Catal.* **130**, 497 (2000).
- Masson, M. J., M.S. thesis, Pennsylvania State University, December 2000.
- Singh, U. K., and Vannice, M. A., *J. Mol. Catal. A* **162**, 287 (2000).
- Kluson, P., and Cerveny, L., *Appl. Catal. A: Gen.* **128**, 13 (1995).
- Touroude, R., *J. Catal.* **65**, 110 (1980).
- Rylander, P. N., "Catalytic Hydrogenation in Organic Synthesis," p. 720 Academic Press, New York, 1979.
- Mercadante, L., Neri, G., Donato, A., and Galvagno, S., *J. Mol. Catal.* **105**, 93 (1996).
- Aramendia, M. A., Borau, V., Jimenez, C., Marinas, J. M., Porras, A., and Urbano, F. J., *J. Catal.* **172**, 46 (1997).
- Sokol'skii, D. V., Pak, A. M., Ginzburg, M. A., and Zavorin, V. A., *Kinet. Katal.* **20**, 645 (1979).
- Tiainen, L.-P., Maki-Arvela, P., and Salmi, T., *Catal. Today* **48**, 57 (1999).
- Delbecq, F., and Sautet, P., *J. Catal.* **152**, 217 (1995).
- Pallassana, V., and Neurock, M., *J. Catal.*, submitted for publication.
- Marinelli, T. B. L. W., Nabuurs, S., and Ponec, V., *J. Catal.* **151**, 431 (1995).
- Pauling, L., *Proc. Roy. Soc. A* **196**, 343 (1949).
- Brunelle, J. P., *Pure Appl. Chem.* **50**, 1211 (1978).
- Palmer, M. B., Jr., and Vannice, M. A., *J. Chem. Tech. Biotechnol.* **30**, 205 (1980).
- van Steen, E., Sewell, G. S., Makhothe, R. A., Micklethwaik, C., Manstein, H., deLange, M., and O'Connor, C., *J. Catal.* **162**, 220 (1996).
- Burattin, P., Che, M., and Louis, C., *J. Phys. Chem. B* **103**, 6171 (1999).
- Jung, H.-J., Vannice, M. A., Mulay, L. N., Stanfield, R. M., and Delgass, W. N., *J. Catal.* **76**, 208 (1982).
- Yoon, K. J., and Vannice, M. A., *J. Catal.* **82**, 457 (1983).
- Singh, U. K., Ph.D. thesis, Pennsylvania State University, August 2000.
- Madon, R. J., and Boudart, M., *Ind. Eng. Chem. Fundam.* **21**, 438 (1982).
- Weisz, P. B., *Z. Phys. Chem.* **11**, 1 (1957).
- de Jesus, J. C., and Zaera, F., *Surf. Sci.* **430**, 99 (1999).
- Brown, N. F., and Barteau, M. A., *J. Am. Chem. Soc.* **114**, 4258 (1992).
- Houtman, C. J., and Barteau, M. A., *J. Catal.* **130**, 528 (1991).
- Davis, J. L., and Barteau, M. A., *J. Am. Chem. Soc.* **111**, 1782 (1989).
- Waghay, A., and Blackmond, D. G., *J. Phys. Chem.* **97**, 6002 (1993).
- Nishiyama, S., Hra, T., Tsuruya, S., and Masai, M., *J. Phys. Chem.* **103**, 4431 (1999).
- Englisch, M., Ranade, V. S., and Lercher, J. A., *Appl. Catal. A: Gen.* **163**, 111 (1997).
- Wrammerfors, A., and Andersson, B., *J. Catal.* **147**, 82 (1994).
- Shekhar, R., and Barteau, M. A., *Surf. Sci.* **319**, 298 (1994).

37. Pradier, C. M., Birchem, T., Berthier, Y., and Cordier, G., *Catal. Lett.* **29**, 371 (1994).
38. Bailie, J. E., Rochester, C. H., and Hutchings, G. J., *J. Chem. Soc. Faraday Trans.* **93**, 4389 (1997).
39. Mavrikakis, M., and Barteau, M. A., *J. Mol. Catal. A: Chem.* **131**, 135 (1998).
40. Davis, J. L., and Barteau, M. A., *Surf. Sci.* **187**, 387 (1987).
41. Sexton, B. A., Rendulic, K. D., and Hughes, A. E., *Surf. Sci.* **121**, 181 (1982).
42. Gates, S. M., Russel, J. N., Jr., and Yates, J. T., Jr., *Surf. Sci.* **171**, 111 (1986).
43. Shekhar, R., and Barteau, M. A., *Catal. Lett.* **31**, 221 (1995).
44. Davis, J. L., and Barteau, M. A., *J. Mol. Catal.* **77**, 109 (1992).
45. Birchem, T., Pradier, C. M., Berthier, Y., and Cordier, G., *J. Catal.* **146**, 503 (1994).
46. Birchem, T., Pradier, C. M., Berthier, Y., and Cordier, G., *J. Catal.* **161**, 68 (1996).
47. Beccat, P., Bertolini, J. C., Gauthier, Y., Massardier, J., and Ruiz, P., *J. Catal.* **126**, 451 (1990).
48. Pallassana, V., Neurock, M., and Coulston, G. W., *J. Phys. Chem. B.* **103**, 8973 (1999).
49. Goodman, D. W., and Xu, C., *Langmuir* **12**, 1807 (1996).
50. Delbecq, F., and Sautet, P., *Catal. Lett.* **28**, 89 (1994).
51. Delbecq, F., and Sautet, P., *Surf. Sci.* **295**, 353 (1993).
52. Fadley, C. S., and Shirley, D. A., "3rd Materials Research Symposium—Electronic Density of States," Nov. 3–6, 1969, Gaithersburg, MD.
53. Nordlander, P., Holloway, S., and Norskov, J. R., *Surf. Sci.* **136**, 59 (1984).
54. Wismeijer, A. A., Kieboom, A. P. G., and van Bekkum, H., *React. Kinet. Catal. Lett.* **29**, 311 (1985).
55. Landis, C. R., and Halpern, J., *J. Am. Chem. Soc.* **109**, 1746 (1987).
56. Englisch, M., Jentys, A., and Lercher, J. A., *J. Catal.* **166**, 25 (1997).
57. Gallezot, P., Giroir-Fendler, A., and Richard, D., in "Chemical Industry 47 (Catalysis of Organic Reactions)" (W. E. Pascoe, Ed.), p. 1. 1992.
58. Butt, J., *AIChE* **22**, 1 (1976).
59. Sinfelt, J. H., *Science* **195**, 641 (1977).